The effects of photoionization on galaxy formation – II. Satellite galaxies in the Local Group

A. J. Benson,[1]★ C. S. Frenk,[2] C. G. Lacey,[3] C. M. Baugh[2] and S. Cole[2]

[1]*California Institute of Technology, MC 105-24, Pasadena, CA 91125, USA*
[2]*Physics Department, University of Durham, Durham DH1 3LE*
[3]*SISSA, Astrophysics Sector, via Beirut 2-4, 34014 Trieste, Italy*

ABSTRACT

We use a self-consistent model of galaxy formation and the evolution of the intergalactic medium to study the effects of the reionization of the Universe at high redshift on the properties of satellite galaxies like those seen around the Milky Way. Photoionization suppresses the formation of small galaxies, so that surviving satellites are preferentially those that formed before the Universe reionized. As a result, the number of satellites expected today is about an order of magnitude smaller than the number inferred by identifying satellites with subhaloes of the same circular velocity in high-resolution simulations of the dark matter. The resulting satellite population has an abundance similar to that observed in the Local Group, although the distribution of circular velocities differs somewhat from the available data. We explore many other properties of satellite galaxies, including their gas content, metallicity and star formation rate, and find generally good agreement with available data. Our model predicts the existence of many as yet undetected satellites in the Local Group. We quantify their observability in terms of their apparent magnitude and surface brightness, and also in terms of their constituent stars. A near-complete census of the Milky Way's satellites would require imaging to $V \approx 20$ and to a surface brightness fainter than 26 V-band magnitudes per square arcsecond. Satellites with integrated luminosity $V = 15$ should contain of order 100 stars brighter than $B = 26$, with central stellar densities of a few tens per square arcminute. Discovery of a large population of faint satellites would provide a strong test of current models of galaxy formation.

Key words: galaxies: formation – intergalactic medium – Local Group – cosmology: theory.

1 INTRODUCTION

High-resolution *N*-body simulations of the formation of dark matter haloes in the cold dark matter (CDM) cosmogony reveal a large number of embedded subhaloes that survive the collapse and virialization of the parent structure (Klypin et al. 1999; Moore et al. 1999). Although their aggregate mass typically represents less than 10 per cent of the total halo mass, these substructures are very numerous. In rich clusters, the abundance of surviving subhaloes is comparable to the abundance of bright galaxies. In galaxy haloes, on the other hand, the number of subhaloes exceeds the number of faint satellites observed in the Local Group by well over an order of magnitude. This discrepancy has recently been highlighted as a major flaw of the CDM cosmogony, and has prompted investigation of alternative cosmological models. These range from non-standard models of inflation (Kamionkowski & Liddle

2000) to models in which the Universe is dominated by warm, self-interacting or annihilating dark matter which may not generate small-scale substructure in galactic haloes, but may do so on cluster scales (Hogan 1999; Moore et al. 2000; Spergel & Steinhardt 2000; Yoshida et al. 2000; Craig & Davis 2001).

That hierarchical clustering theories predict many more small dark matter haloes than there are faint galaxies in the local Universe has been known for a long time, as has one possible solution to this apparent conflict (White & Rees 1978). Feedback generated by the energy injected into galactic gas in the course of stellar evolution can regulate star formation in small haloes, rendering their galaxies too faint to be detected in local surveys (White & Rees 1978; Dekel & Silk 1986; Cole 1991; Lacey & Silk 1991; White & Frenk 1991). The overabundance of dark subhaloes around the Milky Way predicted by CDM models was also known before the high-resolution *N*-body simulations highlighted the discrepancy (Kauffmann, White & Guiderdon 1993). Using a semi-analytic model of galaxy formation based on the extended

★E-mail: abenson@astro.caltech.edu

Press–Schechter theory for the assembly histories of dark haloes (Bond et al. 1991; Bower 1991), Kauffmann et al. recognized the Milky Way 'satellite' problem and examined various possible solutions (see their fig. 1). They concluded that the best way to reconcile their models with the luminosity function of the Milky Way's satellites was to assume that gas is unable to cool within dark matter haloes of circular velocity less than $150 \, \mathrm{km \, s^{-1}}$ at redshifts between 5 and 1.5. They suggested that this effect might result from a photoionizing background at high redshift, but also noted that the required suppression threshold of $150 \, \mathrm{km \, s^{-1}}$ was much larger than was expected based on physical calculations of the effects of photoionization. Moore (2001) has expanded on the reasons why standard supernova feedback of the kind invoked to explain the relative paucity of faint field galaxies in CDM models does not, on its own, solve the Milky Way satellite problem. He points out that the observed satellites of the Milky Way of a given abundance have circular velocities which are about 3 times smaller than the circular velocities of subhaloes of the same abundance in the *N*-body simulations.

The tentative detection of Gunn–Peterson troughs in the spectra of $z \approx 6$ quasars (Becker et al. 2001; Djorgovski et al. 2001) suggests that the Universe reionized at $z \gtrsim 6$. The reionization of the Universe raises the entropy of the gas that is required to fuel galaxy formation, preventing it from accreting on to small dark matter haloes and lengthening the cooling time of that gas which is accreted. The inhibiting effects of photoionization have been investigated in some detail (Rees 1986; Babul & Rees 1992; Efstathiou 1992; Shapiro, Giroux & Babul 1994; Katz, Weinberg & Hernquist 1996; Quinn, Katz & Efstathiou 1996; Thoul & Weinberg 1996; Kepner, Babul & Spergel 1997; Navarro & Steinmetz 1997; Weinberg, Hernquist & Katz 1997; Abel & Mo 1998; Barkana & Loeb 1999), with the conclusion that galaxy formation is strongly suppressed by reionization in haloes of circular velocity, $V_C \lesssim 60 \, \mathrm{km \, s^{-1}}$. Although this value is smaller than the value assumed by Kauffmann et al. (1993), their general picture remains valid: the number of satellites around bright galaxies is much smaller than the number of dark matter subhaloes because only those subhaloes that were already present before reionization were able to acquire gas and host a visible galaxy. This idea has recently been investigated further by Bullock, Kravtsov & Weinberg (2000). These authors followed the formation of dark haloes using a merger tree formalism similar to that of Kauffmann et al. (1993), but taking into account the tidal effects experienced by substructures when they are accreted into their parent halo. Combining their halo model with a simple argument based on the mass-to-light ratio of satellite galaxies, they calculated their observability, concluding that, for a reasonable redshift of reionization, the number of visible satellites would indeed be close to that observed. A similar conclusion has been reached by Somerville (2001) using a semi-analytic model that includes a simplified treatment of photoionization. Her model does not follow the evolution of the galaxies and the IGM in a self-consistent way, and ignores the effects of photoheating of virialized gas in haloes and the tidal disruption of satellites. These turn out to be quite important.

In this paper we investigate the abundance and properties of satellite galaxy populations using a model of galaxy formation which self-consistently calculates the physics of reionization and the process of galaxy formation. We use the semi-analytic techniques developed by Cole et al. (2000), which we have recently extended to enable calculation of the coupled evolution of the intergalactic medium (IGM) and galaxies (Benson et al. 2002, hereafter Paper I). The model follows the formation and evolution

of stars, the production of ionizing photons from stars and quasars, the reheating of the IGM, and the associated suppression of galaxy formation in low-mass haloes. The model also incorporates a detailed treatment of the dynamics of satellite haloes under the influence of dynamical friction and tidal forces (following Taylor & Babul 2001). Like the halo model of Bullock et al. (2000), our model agrees with the results of the high-resolution *N*-body simulations.

In Paper I we demonstrated that reionization reduces the number of faint field galaxies in the local Universe, flattening the faint-end slope of the galaxy luminosity function, in good agreement with the most recent observational determinations. In this paper we explore the properties predicted by this very same model (i.e., with the same parameter values) for the population of satellites around galaxies like the Milky Way. We will carry out as detailed a comparison as is possible with current observational data, and present tests of our model which rely on the prediction of a large and as yet undetected population of faint satellites in the halo of the Milky Way.

The remainder of this paper is organized as follows. In Section 2 we briefly describe our model. In Section 3 we calculate the expected luminosity function and circular velocity function of satellites around galaxies like the Milky Way. In this section we also discuss observational strategies for discovering the large faint satellite population predicted by our model. In Section 4 we compare the gas content, star formation rate, metallicity and structure of our model satellites with observational data. Finally, in Section 5 we present our main conclusions.

2   MODEL

We begin by briefly describing our model, a full description of which may be found in Paper I. We represent the IGM as a distribution of gas elements whose density evolves as a result of the expansion of the Universe and the formation of structure. Each element 'sees' a background of ionizing photons emitted by stars (as given by the star formation history in our model of galaxy formation) and by quasars (as obtained from the observational parametrization of Madau, Haardt & Rees 1999), which ionize and heat the gas. From this, we derive the thermal and ionization history of the IGM. The hot IGM acquires a significant pressure which hampers the accretion of gas into low-mass dark matter haloes. From the inferred thermal state of the IGM we derive the filtering mass, defined as the mass of a dark matter halo which accretes a gas mass equivalent to 50 per cent of the universal baryon fraction (Gnedin 2000), as a function of time.

Knowledge of the filtering mass allows us to determine how much gas is available for galaxy formation in a given dark matter halo at any time. The increase in entropy produced by reionization causes lower mass haloes to contain a smaller fraction of their mass in the form of gas than larger mass haloes. The ionizing background which accumulates after reionization also heats gas already present in dark matter haloes, reducing (sometimes to zero) that rate at which gas cools into the star forming phase. We include this heating in our estimates of the mass of gas which can cool, resulting in a further suppression of galaxy formation. (For particularly cool haloes, photoheating exceeds all cooling processes and the gas is heated above the halo virial temperature. In such cases the gas will never cool to form a galaxy, and instead will be photo-evaporated from the halo as described by Barkana & Loeb 1999.) When a galaxy falls into a larger halo, becoming a satellite in it, we compute its orbit through the halo in detail,

accounting for the effects of dynamical friction, tidal limitation and gravitational shocking (as described by Taylor & Babul 2001 and in Paper I). As was demonstrated in Paper I, our model of satellite dynamics reproduces the results of high-resolution *N*-body simulations with reasonable accuracy in both of the cosmological models for which numerical results are available.

In Paper I we performed calculations using our extended galaxy formation model in a ΛCDM cosmology (mean mass density $\Omega_0 = 0.3$, cosmological constant term $\Lambda/3H_0^2 = 0.7$, mean baryon density $\Omega_b = 0.02$, and Hubble parameter $h = 0.7$). The values of the model parameters required to describe the relevant physical processes are strongly constrained by a small subset of the local galaxy data; we showed that the model also reproduces many other properties of the galaxy population at $z = 0$ (see also Cole et al. 2000). We will retain exactly the same parameter values throughout the present work. The result is a fully specified model of galaxy formation that incorporates the effects of reionization and tidal limitation, and which we now use to explore in detail the properties of satellite galaxies around the Milky Way.

3 THE ABUNDANCE OF SATELLITES

We study the population of satellite galaxies that form in an ensemble of haloes harbouring galaxies similar to the Milky Way. We class a galaxy as being 'similar to the Milky Way' if the circular velocity of its disc ($V_{C,d}$, measured at the disc half-mass radius) is between 210 and $230 \, \mathrm{km \, s^{-1}}$, and if its bulge-to-total mass ratio (including stars and cold gas) is in the range 0.05 to 0.20 (which is approximately the range found by Dehnen & Binney 1998 in mass models of the Milky Way).

Using our model of galaxy formation, including all the effects of photoionization and tidal limitation described in Section 2, we construct 1800 realizations of dark matter haloes with mass in the range 4.0×10^{11} to $2.3 \times 10^{12} \, h^{-1} \, M_\odot$ (the range in which we find galaxies similar to the Milky Way) at $z = 0$. (We pick halo masses to produce a uniform distribution of the logarithm of halo mass in this range.) We ensure that our calculation resolves all haloes into which gas is able to accrete and cool in the redshift interval 0 to 25. From the set of simulated haloes we select those which contain a central galaxy similar to the Milky Way. We find approximately 70 such haloes in our sample (the fraction of haloes hosting Milky Way galaxies is higher near the centre of the mass range considered and significantly lower towards the extremes). This number, of course, depends on the precise range of circular velocity and bulge-to-total ratio that we use to define Milky Way-like galaxies. Our results are quite insensitive to these choices – doubling the allowed range of circular velocities for example makes no significant difference to the satellite luminosity and velocity functions derived below. The haloes so selected have 'quieter' merger histories than is typical for haloes of their mass, as was shown, for example, by Baugh, Cole & Frenk (1996). If we had selected haloes in the same range of circular velocity but with bulge-to-total ratios characteristic of elliptical galaxies, the number of satellite galaxies would have been larger by around 40 per cent at faint magnitudes. All other haloes are discarded and, for the remainder of this paper, we consider only the satellite populations of haloes hosting Milky Way-type galaxies. We refer to this sample of satellites as our 'standard model.' For comparison, we also generated a sample of Milky Way satellites using our model with no photoionization (but still including the effects of tidal limitation of satellites), which we will refer to as the 'no photoionization' model, and a sample of Milky Way satellites with the original model of Cole et al. (2000), which includes neither photoionization nor tidal effects. Our model results depend upon the fraction of ionizing photons produced in galaxies which are able to escape into the IGM, f_{esc}. We will follow Paper I and present results for $f_{esc} = 10$ and 100 per cent.

To test our model, we make use of observational data on Local Group galaxies taken from the compilation by Mateo (1998). Mateo points out that the census of Local Group dwarfs is almost certainly incomplete. Unfortunately, the observational selection effects are not well understood quantitatively, and so we do not attempt to correct for them here, but note that they could possibly alter the observational results significantly. Some galaxies classed as members of the Local Group lie outside the virial radii of the dark matter haloes thought to be associated with the Milky Way and M31. For the Milky Way, we can estimate the virial radius using the three-component mass models of Dehnen & Binney (1998), some of which assume dark matter haloes with the NFW (Navarro, Frenk & White 1997) profile appropriate to the CDM universe that we are considering here. Of these, their model 2d gives the best fit to the observational data that they consider. Assuming a spherical top-hat collapse model for the Milky Way halo then implies a virial mass and radius of $M_{MW} = 1.11 \times 10^{12} \, M_\odot$ and $R_{MW} = 272 \, \mathrm{kpc}$ respectively (for the particular set of cosmological parameters considered in this paper). This is in good agreement with the virial radii of the haloes that end up hosting Milky Way-type galaxies in our model, which typically have $R_{vir} \approx 300 \, \mathrm{kpc}$. (The model predicts a distribution of R_{vir} because Milky Way-type galaxies can be found in haloes with a range of masses.) Lacking any better estimate, we also take R_{MW} as the virial radius of M31, since the measured circular velocity of M31 is quite close to that of the Milky Way. Throughout this section, we will distinguish between Local Group satellites and satellites lying within R_{MW} of either the Milky Way or M31.

3.1 Abundance as a function of luminosity and stellar mass

We begin by comparing the luminosity function of the population of satellites in the model with the observed luminosity function of satellites of the Local Group. In Fig. 1 we plot as filled circles the observed *V*-band luminosity function of satellites,[1] normalized to the number of central galaxies (i.e., the Milky Way and M31). We include only satellites within R_{MW} of either the Milky Way or M31. (In this respect we differ from Somerville 2001, who included all Local Group members. Since our model, as well as Somerville's, is intended to predict only the population of satellites within the Milky Way halo, it is important to use the equivalent set of observational data in order to make a fair comparison. Including all of the Local Group galaxies overestimates the luminosity function of the Milky Way's satellites by a factor of 1.8 on average.) Throughout this paper, we use magnitudes corrected for foreground extinction by the Milky Way using the reddening values listed by Mateo (1998). The incompleteness of the Local Group sample is exposed by the fact that the more recent compilation by Irwin[2] contains four satellites not included in Mateo's sample. Three of these lie within the virial radius of M31, indicating that the incompleteness is probably greater for M31 than for the Milky Way system, as might be expected, given the greater distance of M31. These satellites are included in the observational sample used to construct Fig. 1.

The bottom panel of Fig. 1 compares the predicted luminosity

---

[1] We include the SMC, LMC and M33 in this category.
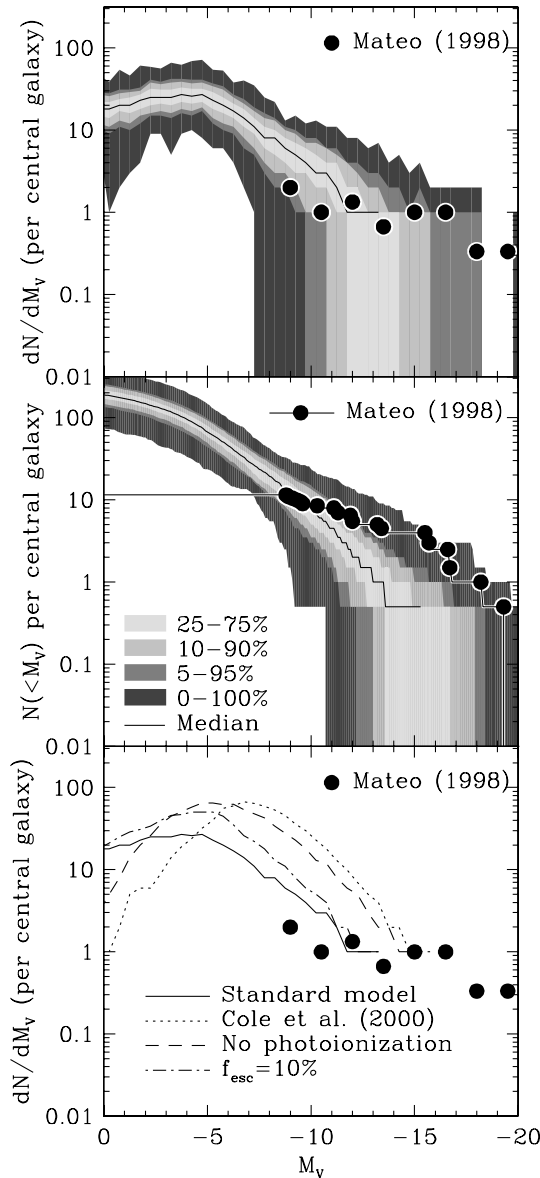[2] http://www.ast.cam.ac.uk/~mike/local_members.html

Figure 1. The *V*-band luminosity function of satellite galaxies (per central galaxy) is shown in differential (top and bottom panels) and cumulative (middle panel) forms. The Local Group data, taken from the compilation of Mateo (1998), and supplemented by data from Irwin, are shown as filled circles. (Faintwards of $M_V = -9$ there are no known satellites, so we plot no symbols.) Only satellites within $R_{\rm MW}$ of the Milky Way or M31 are included, and no correction for any possible incompleteness has been applied. *Top panel:* The solid line shows the median *differential* luminosity function of satellites around pairs of Milky Way-type galaxies in our model for $f_{\rm esc} = 100$ per cent. The shaded regions show intervals around the median, according to the key in the middle panel. (Note that 0–100 per cent interval is not a stable statistical quantity, but is shown to illustrate the most extreme examples found in our sample of 70 Milky Way-type haloes.) *Middle panel*: The solid line shows the median *cumulative* luminosity function of satellites around pairs of Milky Way-type galaxies in our model, while the shaded regions show intervals around the median, as in the top panel. *Bottom panel:* A comparison of the *differential* luminosity functions predicted for different model assumptions. The solid line shows the median luminosity function from our standard model, and the dot-dashed line the results from our model with an escape fraction of $f_{\rm esc} = 10$ per cent. The dashed line corresponds to the model in which the effects of photoionization are ignored (but tidal limitation of satellites is included), while the dotted line shows the prediction from the model of Cole et al. (2000). (Note that no lines are plotted where the median drops to zero.)

function from our standard model with that from the model of Cole et al. (2000), and also with a model which includes tidal stripping but not the effects of photoionization. It is immediately apparent that our new model predicts many fewer satellites than the Cole et al. model and, furthermore, that this is mostly a consequence of photoionization, tidal stripping having a much smaller effect. For $M_V \approx -10$, the combined effects of tidal stripping and photoionization reduce the number of satellites by about a factor of 10 compared to the Cole et al. model.

The top and middle panels of Fig. 1 compare the luminosity function predicted by our model with $f_{\rm esc} = 100$ per cent with the observational data. The comparison is made in terms of the differential luminosity function in the top panel, and the cumulative luminosity function in the middle panel. In both panels, the solid line shows the median luminosity function from all pairs of Milky Way-type galaxies in our model, while the shaded regions show intervals around the median. (We calculate the median and intervals for pairs of haloes, since we are comparing to the combined Milky Way and M31 datasets, and the scatter in model predictions for pairs of haloes is, of course, smaller than for single haloes.) The satellite galaxies in our model typically have only very small amounts of internal dust-extinction (all but a tiny fraction have less than 0.1 magnitudes of extinction in the *V* band). Nevertheless, we include the effects of internal dust-extinction in all model magnitudes.

As is apparent from the width of the shaded region in Fig. 1, the model predicts significant variations in the satellite luminosity function from halo to halo. Once this scatter is taken into account, the Local Group data fall within the range predicted by the model, except perhaps at the brightest magnitudes, where the model seems to predict too few satellites. However, the observational statistics are poor at these magnitudes, because there are so few galaxies. For example, the $-17.25 \geq M_V > -18.75$ bin in Fig. 1 contains a single galaxy (the LMC) within $R_{\rm MW}$, implying a mean of 0.5 such satellites per central galaxy. As may be seen in the figure, such galaxies are found in $\lesssim 5$ per cent of model haloes, making them rare, but not non-existent.

Although the observational data fall within the range spanned by the models, it is important to realize that no single pair of model haloes has a luminosity function as flat as that found observationally. This is clearly seen when the data are plotted in cumulative form, as in the middle panel of Fig. 1. This plot shows that the median prediction for the total number of satellites brighter than $M_V = -9$ is in excellent agreement with the observations, but also that the model haloes typically have much steeper luminosity functions than the Milky Way/M31 system, with fewer than 5 per cent of model haloes producing as many of the brightest satellites as are observed locally.

As was noted in Paper I, the disc velocity dispersion used in the Taylor & Babul (2001) model ($\sigma_{\rm d} = V_{\rm C,d}/\sqrt{2}$) is rather high for the Milky Way. This quantity determines the magnitude of the dynamical friction force felt by satellites which pass close to the disc of the central galaxy, and so may affect the rate of merging for satellites on highly eccentric orbits. An overly large $\sigma_{\rm d}$ would result in reduced dynamical friction and a lower rate of mergers, potentially causing us to overestimate the number of satellites remaining. However, adopting the value $\sigma_{\rm d} = 0.2 V_{\rm C,d}$ (which results in a 1D velocity dispersion of approximately 30 to $40 \, {\rm km \, s^{-1}}$, similar to that observed for the Milky Way) makes virtually no difference to the predicted number of satellites, since the disc velocity dispersion is important only for satellites passing very close to the central galaxy and which tend to merge shortly

afterwards in any case. Similarly, adopting the Bullock et al. (2001) method of fixing dark matter halo concentrations instead of the Navarro et al. (1997) method normally employed in this work results in only a 10–20 per cent reduction in the number of satellites (brightwards of the peak in the luminosity function; at fainter magnitudes there is a slight increase in the number of satellites). On the other hand, the abundance of the faintest satellites is fairly sensitive to two uncertain model assumptions, the escape fraction of ionizing photons, f_{esc}, and the luminosity of the galaxies that we have classed as resembling the Milky Way.

In Paper I we found that adopting an escape fraction, $f_{esc} = 100$ per cent (i.e., all ionizing photons produced by stars escape from their galaxy into the IGM) gives the ionizing emissivity at $z \approx 3$ from Lyman-break galaxies and results in a redshift of reionization $z \approx 8$, but also in an ionizing background which is significantly higher than current observational estimates. On the other hand, a fraction $f_{esc} = 10$, per cent, results in a more reasonable ionizing background and is in better agreement with observational determinations of f_{esc} (Leitherer et al. 1995; Steidel, Pettini & Adelberger 2001), but implies a lower redshift of reionization ($z \approx 5.5$) which is slightly too low compared to observational data. Recent observational estimates (Becker et al. 2001; Djorgovski et al. 2001) put the redshift of reionization at $z \gtrsim 6$, intermediate between our two models. We find that the lower redshift of reionization associated with $f_{esc} = 10$ per cent leads to a larger number of satellites of a given luminosity (as shown by the dot-dashed line in Fig. 1), producing a luminosity function which, faintwards of $M_V = -11$, is around 50 per cent higher than the $f_{esc} = 100$ per cent model and thus somewhat too high compared with the data (even after allowing for halo-to-halo variations). However, possible incompleteness at the faint end of the observed luminosity function makes this comparison inconclusive. We will show results for $f_{esc} = 100$ per cent unless stated otherwise. In Paper I we noted that the contribution of quasars to the ionizing emissivity of the Universe was important in determining the low-z behaviour of our model. As an extreme example, we find that ignoring this contribution entirely results in only a small increase in the number of satellites for the $f_{esc} = 100$ per cent case (since here the reionization of H I is driven almost entirely by the stellar emissivity), but has a larger effect for $f_{esc} = 10$ per cent (in this case the satellite galaxy luminosity function is increased by approximately 15 per cent at $M_V = -5$, with a lesser effect at brighter magnitudes).

A second source of uncertainty is the identification of model galaxies with the Milky Way. As discussed in Paper 1 (see fig. 9), our modelling of the structure of discs is crude and produces circular velocities for spiral galaxies that are typically 30 per cent larger for their luminosity than is implied by the observed Tully–Fisher relation. As a result, the model galaxies that we have identified with the Milky Way according to their circular velocity are somewhat fainter than galaxies lying on the mean Tully–Fisher relation at that circular velocity. We could alternatively select Milky Way galaxies according to luminosity. Direct estimates of the luminosity of the Milky Way are rather uncertain, and so we instead estimate the luminosity from the observed Tully–Fisher relation, as advocated by Binney & Merrifield (1998, section 10.1). The observed Tully–Fisher relation (Matthewson, Ford & Buchhorn 1992) implies an I-band magnitude in the region of $-21.5 \gtrsim M_I - 5 \log h \gtrsim -22.0$ for a typical galaxy with the circular speed of the Milky Way. Model galaxies with I-band magnitude in this range (and bulge-to-total ratio in the range discussed above) typically have higher circular velocities, and

inhabit higher mass haloes than the Milky Way-type galaxies of our original sample. As a result, this new sample has a substantially larger number of satellites. Its luminosity function is compatible with observations for magnitudes brighter than $M_V \approx -13$, but faintwards of this, it overpredicts the number of satellites. Again, possible incompleteness in the faint data makes it difficult to exclude this model, but for it to be compatible with observations, the data would have to be severely incomplete so that at least 70 per cent of $M_V \approx -10$ satellites should have been missed.

3.2 Predicted number of very faint satellites

As can be clearly seen from Fig. 1, our model predicts that the satellite galaxy luminosity function should continue to rise at magnitudes fainter than the faintest satellite yet observed. The luminosity function peaks at $M_V \approx -3$ and then falls off at fainter magnitudes. This cut-off is caused by the inability of gas below 10^4 K to cool when no molecular hydrogen is present. The cut-off occurs at significantly fainter magnitudes in our standard model than in the model with no-photoionization or the Cole et al. (2000) model, since photoionization reduces the efficiency of galaxy formation in haloes of a given mass (or, equivalently, virial temperature) making the galaxies in those haloes fainter.[3] It is interesting therefore to consider the observability of the galaxies that make up the faint end of the satellite luminosity function. In Fig. 2 we show the cumulative number of satellite galaxies per halo as a function of their V-band apparent magnitude. To infer the distances to the satellites, we have made use of their orbital positions, assuming that they are observed from a location 8 kpc from the centre of the host halo (i.e., at about the position of the Sun in the Milky Way). (The mean distance for $M_V \leq -10$ satellites is 95 kpc, and this changes only slowly with M_V.)[4] The solid line shows all satellites, while the dotted and dashed lines show only those whose central surface brightness is brighter than 26 and 22 mag arcsec^{-2} respectively. Central surface brightness for model galaxies were computed using the predicted luminosities and sizes, with disc components modelled as exponential discs, and spheroids as King profiles with $r_t/r_c = 10$. For comparison, the faintest known Local Group galaxy is Tucana, with $m_V = 15.15$ (note that this point is not seen in Fig. 2, since Tucana lies outside of the Milky Way's virial radius). Surface brightness adds a further limit to the detectability of satellites. Currently, the lowest surface brightness member of the Local Group that is known is Sextans, with $\mu_0 = 26.2 \pm 0.5$ mag arcsec^{-2} (Mateo 1998). This is similar to the surface brightness limit for the dotted line in Fig. 2. It is clear from Fig. 2 that the faint satellites have very low surface brightness, and that finding them will require very deep photometry.

Several satellites have now been detected as an excess of stars against the background of the Milky Way (e.g. Irwin &

---

[3] We are able to predict the properties of these very faint galaxies by extrapolating our standard rules for star formation, feedback, etc. to these very small objects. However, it should be kept in mind that these very faint galaxies typically contain only a few thousand solar masses of stars. It is not clear how well our simplified rules for star formation describe reality in such systems, where the entire galaxy is less massive than a single giant molecular cloud.

[4] The number density of satellites within the virial radius of a Milky Way-type halo in our model scales roughly as r^{-2} for $r \gtrsim 10$ kpc, with a rapid cut-off towards R_{vir}, but flattens significantly at smaller radii, since these inner satellites are strongly affected by tidal forces and dynamical friction.
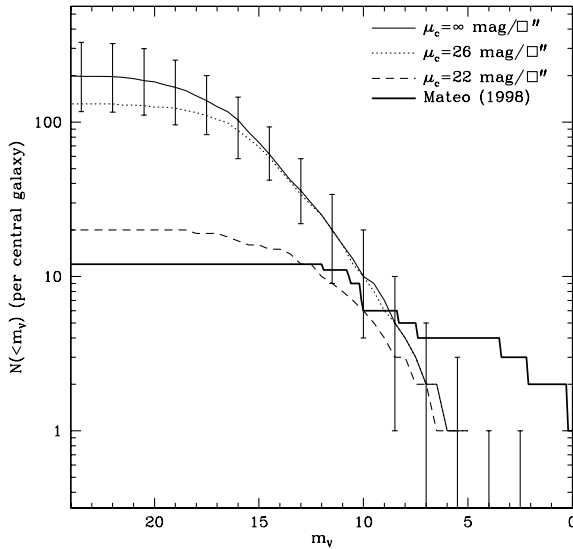
Figure 2. Predicted cumulative number counts of satellites in the *V* band. The solid line shows the median counts from our standard model with no cut on central surface brightness, while the dotted and dashed lines show the effects of applying central surface brightness cuts of 26 and 22 mag/arcsec^{-2} respectively. The error bars indicate the 10 and 90 per cent intervals of the distribution for the results with no surface brightness cut. Note that, unlike the luminosity function plotted in Fig. 1 the results here refer to a single halo (rather than a pair of haloes). Apparent magnitudes for satellites in the model are computed from their position in the host halo, assuming that the observer is located 8 kpc from the centre. The heavy solid line shows the observed counts from Mateo (1998), including only those galaxies within R_{MW} of the Milky Way.

Hatzidimitriou 1995). From the star formation histories of our model satellites, we can calculate the number and surface density of stars visible today. We use the stellar evolutionary tracks of Lejeune & Schaerer (2001) to obtain the number of stars brighter than a certain luminosity, L_C, in a single stellar population of unit mass, as a function of age and metallicity:

$$N_{L_c}(t, Z) = \int_{M_{min}}^{M_{max}} S_{L_c}(M, t, Z) \frac{dn}{dM} dM, \qquad (1)$$

where dn/dM is the stellar initial mass function (IMF; we use the IMF of Kennicutt 1983, as assumed in our calculations of galaxy luminosities), normalized to unit mass and with minimum and maximum masses, M_{min} and M_{max} (0.1 and 125 $M_{\odot}$ respectively), and

$$S_{L_c}(M, t, Z) = \begin{cases} 0 & \text{if } L(M, t, Z) < L_c \\ 1 & \text{if } L(M, t, Z) \geq L_c, \end{cases} \qquad (2)$$

where $L(M, t, Z)$ is the luminosity of a star of zero-age mass M, age t and metallicity Z. The number of stars more luminous than L_c in a galaxy at the present day is then given by

$$N = \int_0^{t_0} \dot{\rho}_{\star}(t) N_{L_c}[t_0 - t, Z(t)] dt, \qquad (3)$$

where $\dot{\rho}_{\star}(t)$ is the star formation rate in the galaxy at time t, and $Z(t)$ is the metallicity of the stars being formed at time t. For each satellite, we compute the luminosity corresponding to a given apparent magnitude limit at its position in the halo, and determine N. From the known size of the disc and spheroidal component of each model galaxy, we also derive the central number density of
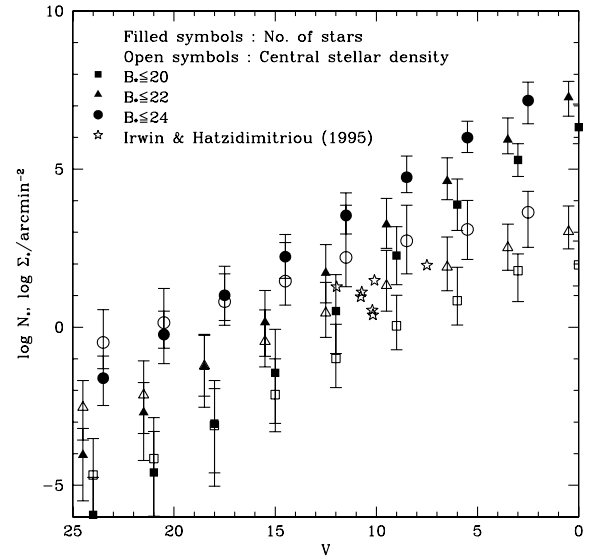

Figure 3. The number of stars (filled symbols) and the surface density of stars (open symbols) brighter than $B_{\star} = 20$, 22 and 24 (squares, triangles and circles respectively) for satellites of Milky Way-type galaxies as a function of the apparent magnitude of the galaxy. The measured central stellar densities for a subset of the Local Group satellites measured by Irwin & Hatzidimitriou (1995), with a limiting magnitude $B = 22$, are shown as open stars.

these stars. Fig. 3 shows the result of this calculation. (We do not include the effects of dust extinction on the stellar luminosities, since this varies across the galaxy, but we do include them in the total galaxy magnitude. As noted above, these internal extinction corrections are typically small in any case.) The central stellar densities predicted by our model are in excellent agreement with those measured by Irwin & Hatzidimitriou from scanned photographic plates with a limiting magnitude of $B = 22$: compare the open stars with the open triangles in Fig. 3. Imaging two magnitudes deeper (circles) would allow the detection of galaxies to $V = 17-18$ at the same central surface density, although the higher density of background objects may make detection more difficult.

3.3 Abundance as a function of circular velocity

In this subsection we derive the abundance of model satellites as a function of their circular velocity and compare it to the Local Group data. This is the statistic originally employed by Klypin et al. (1999) and Moore et al. (1999) to highlight the apparent discrepancy between the CDM cosmogony and the properties of the satellites of the Milky Way. Their motivation for using the distribution of circular velocities of satellite haloes is that it can be straightforwardly obtained from *N*-body simulations including only dark matter, whereas the luminosities of satellite galaxies, while fairly easy to measure observationally, cannot be so easily predicted theoretically because of the complicated dependence on the processes of cooling, star formation, feedback and photo-ionization. The main drawback of making the comparison in terms of circular velocities is that measuring circular velocities is a difficult task for the majority of the Local Group satellites which do not have gas discs, and in any case these measurements give the circular velocity within the visible galaxy, not the value at the peak of the rotation curve of the dark halo, which is typically what is measured in the simulations. In addition, the comparisons by

Klypin et al. (1999) and Moore et al. (1999) implicitly assumed a tight relation between subhalo circular velocity and satellite luminosity. However, the observational selection on luminosity modifies the form of the circular velocity distribution, as we will see below.

Before proceeding with the calculation of the satellite circular velocity distribution, it is important to check that our model produces realistic sizes for the satellites, as well as the correct luminosity–circular velocity relation. The size of a galaxy influences the circular velocity, because it determines the self-gravity of the visible component (and the associated compression of the halo which we treat using adiabatic invariants, as discussed in Cole et al. 2000). It also determines the part of the rotation curve
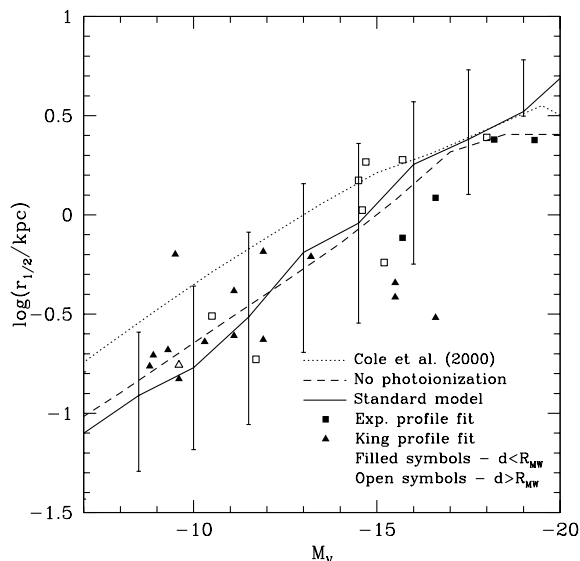
Figure 4. The half-light radii of satellite galaxies as a function of absolute *V*-band magnitude. The points show the radii of the satellites of the Local Group, estimated from the data compiled by Mateo (1998). For spiral and irregular galaxies, we convert their measured exponential scalelength, r_{exp}, to a half-light radius by assuming an exponential disc density profile, $r_{1/2} \approx 1.68 r_{exp}$; we show these points as squares. For ellipticals and dwarf spheroidals, we use the quoted parameters of the King (1966) model fits to reconstruct the density profile of the galaxy, and so infer the half-light radius. The core and tidal radii listed by Mateo are measured along the major axis of each galaxy. We replace these with the equivalent radii for spherically symmetric systems by computing the geometric mean of the radii along the semimajor and semiminor axes (using the measured ellipticities, which we assume to be independent of radius). These points are shown as triangles. (In the few cases where a galaxy is classed as Irr/dSph, we include it in the Irr class for the purpose of this plot.) Filled points indicate satellites within a distance $R_{MW} \approx 270$ kpc from the Milky Way or M31, and open symbols indicate more distant satellites. The solid line corresponds to our standard model, the dashed line to the model that ignores photoionization but which includes tidal stripping of satellite haloes, and the dotted line to the Cole et al. (2000) model. The lines show the median relation and the error bars indicate the 10 and 90 per cent intervals of the distribution in the standard model. In this and subsequent figures, error bars are shown only where the magnitude bin contains enough model galaxies to estimate the 10 per cent and 90 per cent intervals accurately, and so do not appear at the brightest magnitudes. The scatter in the no-photoionization model is similar to this, but in the Cole et al. model it is typically 60–70 per cent of the standard model scatter. The half-light radius of the model satellites is taken to be the half-mass radius of the galaxy (including both disc and spheroid) remaining within the effective tidal radius. The half-mass radii of the disc and spheroid prior to tidal limitation were determined in the manner described by Cole et al.

that is accessible to observations. The luminosity–circular velocity relation enters because, in practice, the distribution of circular velocity is measured for a sample selected to be brighter than a given luminosity.

In Fig. 4 we compare the half-light radii of our model satellites with observations. We estimate the half-light radii of real satellites using published fits to their surface brightness profiles (typically exponentials or King models) in the manner described in detail in the figure caption.[5] For the model satellites, we take the half-light radius to be the half-mass radius of the stellar system (including both disc and spheroid) that remains within the effective tidal radius. (In Paper I we defined the effective tidal radius as the radius in the original satellite density profile beyond which material has been lost.) We show results for our standard, no-photoionization and Cole et al. (2000) models. The sizes of satellites in our standard model are significantly smaller than in the Cole et al. model, particularly at magnitudes fainter than $M_V = -15$. As the figure shows, much of this reduction is due to tidal limitation which strips away the outer layers of the galaxies. Photoionization appears to have little effect on the sizes of satellites. In reality, photoionization does reduce the size, but it also reduces the luminosity, essentially preserving the size–luminosity relation, so that the galaxies typically move in a direction almost parallel to the median relation in Fig. 4. The model predictions are in good agreement with the data and, given the rather crude observational determinations available, this level of agreement seems sufficient at present.

The 'Tully–Fisher' relation between the circular velocity and the *V*-band absolute magnitude of satellites is plotted in Fig. 5. Whenever possible, the circular velocity of real satellites was estimated from the rotation velocity of gas in the ISM (corrected for inclination). Where a measurement of this is not available, we used instead the measured stellar velocity dispersion multiplied by a factor of $\sqrt{3}$.[6] For the model satellites, we plot the circular velocity at the stellar half-mass radius, which is typically ~ 25 per cent smaller than the peak circular velocity in the tidally limited halo. For the fainter satellites ($M_V \simeq -10$), the circular velocity at the half-mass radius is about half the value at the virial radius, whereas for the brighter satellites ($M_V \simeq -15$), the two are similar. The theoretical relations provide a reasonably good description of the data, except in the magnitude range $-9 \lesssim M_V \lesssim -14$ for which the model velocities are about a factor of 2 too high. In this range, the no-photoionization model performs slightly better than the standard model, since tidal limitation results in the rotation velocity being measured at a smaller radius, an effect

which is offset by the fact that photoionization requires galaxies of fixed luminosity to form in more massive haloes when photoionization is switched on (compare the solid and dashed lines in Fig. 5). While it is possible that this discrepancy may reflect a shortcoming of the model, the estimation of circular velocities from current observational data is highly uncertain; improved determinations are extremely important. In addition, there is also some theoretical uncertainty in the calculation of the circular velocity. For example, as noted in Paper I, our model does not account for changes in the density profile of the satellite after tidal limitation, which may reduce the rotation speed somewhat (Mayer et al. 2001). At higher values of V_C (i.e., above $50 \, \mathrm{km \, s^{-1}}$) the agreement between model and data appears to be very good. For field galaxies we find an offset of approximately 1.5 mag between model and data at $V_C = 100 \, \mathrm{km \, s^{-1}}$ (see fig. 11 of Paper I). The model prediction for the satellite galaxy Tully–Fisher relation is very close to that for field galaxies at these velocities. The Local Group data are somewhat fainter than the median of the field galaxy Tully–Fisher relation if we include all Local Group galaxies, thus explaining the apparently better agreement with the model prediction. However, if we restrict our attention to those Local Group satellites with $d < R_{MW}$ and with directly measured rotation velocities (for which the comparison to the model is most secure), we see that the model galaxies are too faint (by around 1 mag) at $V_C \approx 100 \, \mathrm{km \, s^{-1}}$. Of course, the number of such galaxies is rather small, so it is difficult to draw a firm conclusion.
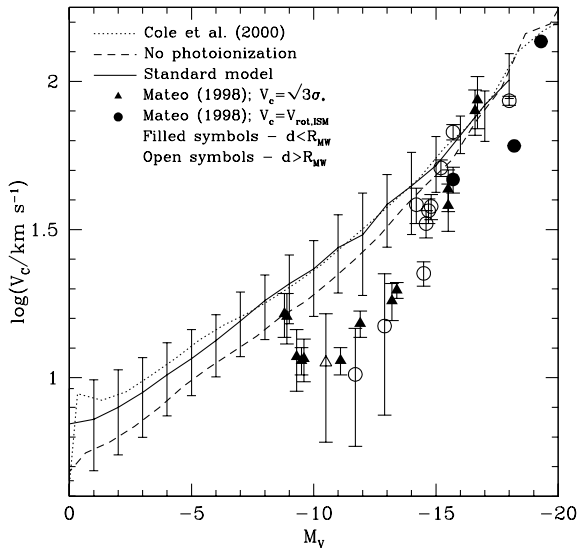

Figure 5. The relation between circular velocity *V*-band absolute magnitude for satellite galaxies. For the real satellites of the Local Group (Mateo 1998), circles indicate circular velocities inferred from the rotation speed of the ISM, while triangles indicate circular velocities estimated from the stellar velocity dispersion as discussed in the text. Filled symbols denote galaxies within R_{MW} of the Milky Way or M31, while open symbols denote more distant galaxies. The median relation from our standard model is shown by the solid line with error bars indicating the 10 and 90 per cent intervals of the distribution. For the model, we plot the circular velocity at the half-mass radius of the satellite (including both disc and spheroid, and taking only the mass remaining within the effective tidal radius). The dashed line shows the results from the model in which the effects of photoionization are ignored, but tidal limitation of haloes is included, while the dotted line shows the results from the model of Cole et al. (2000). The scatter in the former is similar to that in the standard model, but in the latter it is about 70 per cent of that in the standard model.

The cumulative velocity distribution of satellites is shown in Fig. 6. In our model of photoionization, every dark matter halo whose virial temperature is larger than the minimum temperature for cooling (see fig. 1 of Paper I) forms a galaxy (although in low-mass haloes the galaxies have extremely low mass), and tidal stripping never completely destroys a satellite halo (although haloes may be stripped to very small radii). As a consequence, if we naively constructed the full cumulative velocity function of satellites in our model, it would be almost identical to that of the model of Cole et al. (2000). In reality, many of the satellites in our model are extremely faint, either because photoionization severely restricted their supply of star-forming gas, or because tidal stripping removed most of their stars, and so would be unobservable. We therefore apply an absolute magnitude limit to our sample of satellites, and construct the cumulative velocity function only for galaxies brighter than this limit. The sample of known Local Group satellites does not have a well-defined absolute magnitude limit (nor an apparent magnitude limit for that matter), but the faintest galaxy listed by Mateo (1998), Draco, has $M_V = -8.8$. We therefore choose $M_V = -9$ as a suitable cut for our models and apply the same cut to the data.

In the upper left-hand panel of Fig. 6 we show the prediction of our standard model. The median result is indicated by the thin solid line, while the shaded regions show intervals of the distribution around the median. The scatter from realization to realization is large: the central 80 per cent of the distribution of velocity functions spans a factor of 3 in number at a given circular velocity. At low V_C, the total number of satellites predicted agrees well with the observational data but, as we already saw in the case of the luminosity function, the shape of the velocity function differs from that of the data in the sense that the model predicts too few of the highest V_C galaxies. Fewer than 5 per cent of pairs of model haloes contain as many galaxies with $V_C > 40 \, \mathrm{km \, s^{-1}}$ as are observed in the Milky Way/M31 system.

Of the 23 known satellites within the virial radii of the Milky Way or M31 (including the new satellites from the Irwin compilation), only 16 have measured rotation speeds or velocity dispersions, rendering the observational data plotted in Fig. 6 incomplete. To estimate the effects of this incompleteness, we assigned satellites with no measured circular velocity the mean value for galaxies of their luminosity (using the data of Fig. 5), and show the resulting cumulative velocity function as the dashed line in the upper left-hand panel of Fig. 6. The effect is to increase the velocity function by a factor of about 1.2–1.5, while making little difference to its shape. Since the effect of this incompleteness correction is modest, we compare with the uncorrected data in what follows.

The upper right-hand panel of Fig. 6 compares the predicted velocity distributions for our standard model, the Cole et al. (2000) model, and a model including tidal effects but no-photoionization. It is immediately apparent that while the Cole et al. model substantially overpredicts the number of satellites, our photoionization model is in much better agreement with the total number of observed satellites. As the figure clearly shows, at low V_C the main reduction in the number of satellites comes from the effects of photoionization; tidal limitation alone has only a minor effect. However, at $V_C \gtrsim 30 \, \mathrm{km \, s^{-1}}$, tidal stripping becomes the dominant effect in reducing the number of satellites below the prediction of the Cole et al. model. Thus the effects of tidal limitation are crucial for understanding the velocity function at the largest circular velocities, where the model disagrees most significantly with the data. Our results are weakly dependent on the assumed
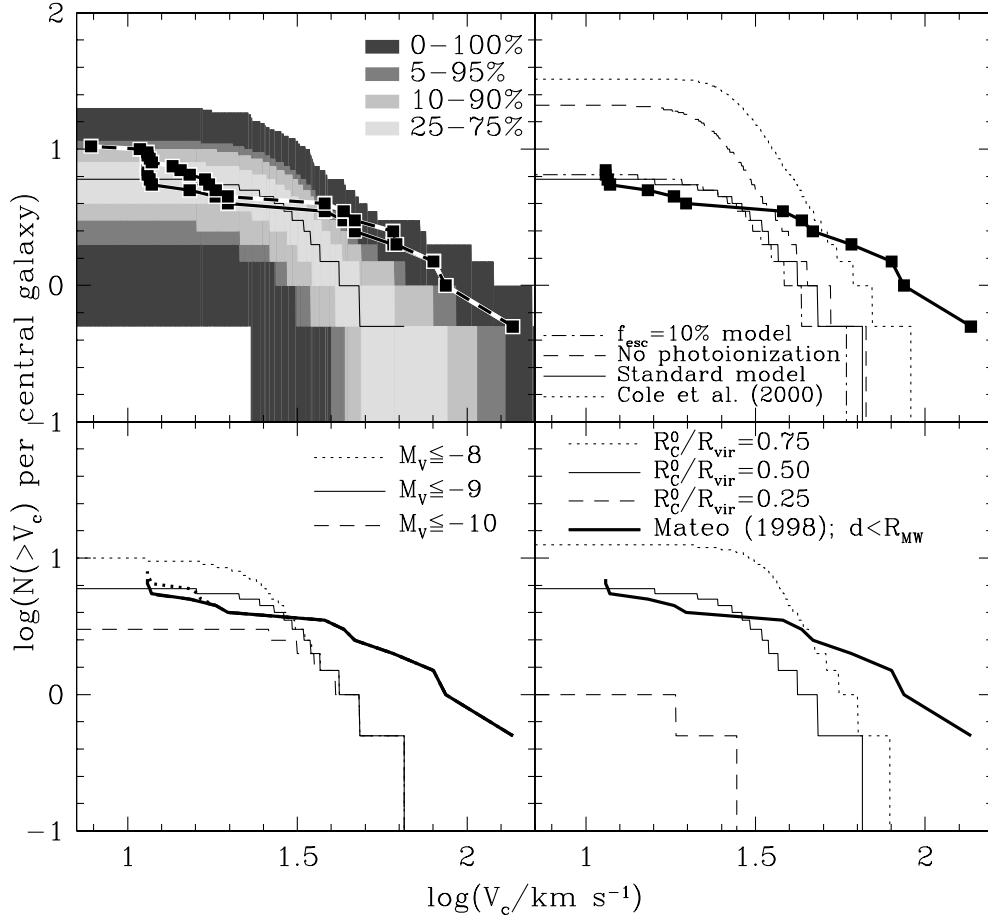
Figure 6. The cumulative velocity function of satellite galaxies. Observational data for the Local Group per central galaxy (i.e., satellites within R_{MW} of the Milky Way or M31), taken from Mateo (1998), are plotted as heavy lines without error bars. (In the upper panels we also plot squares to indicate the contribution from each individual satellite.) In the upper left-hand panel only, we also show the observed velocity function corrected for satellites with no measured circular velocity, as described in the text. *Upper left-hand panel:* the cumulative velocity function of satellites brighter than $M_V = -9$ in our standard model. The thin solid line shows the median velocity function while the shaded regions show intervals of the distribution around the median, as indicated in the panel. (Note that the 0–100 per cent interval is not a stable statistical quantity, but is shown to illustrate the most extreme examples found in our sample of 70 Milky Way-type haloes.) The circular velocities plotted are measured at the half-mass radius of the combined disc and spheroid system after accounting for tidal limitation. *Upper right-hand panel:* the median cumulative velocity function of satellites brighter than $M_V = -9$ in our standard model (solid line). The dot-dashed line shows the effect of reducing f_{esc} to 10 per cent (from 100 per cent in the standard model). The dashed line shows the model in which the effects of photoionization are neglected, but satellite limitation by tidal stripping is included, while the dotted line shows the model of Cole et al. (2000). All models have $R_c^0/R_{vir} = 0.5$. *Lower left-hand panel:* dependence on the absolute magnitude cut. The thin lines show results for the standard model for the different magnitude cuts: solid for $M_V = -9$ (as in the upper panels), dotted for $M_V = -8$, and dashed for $M_V = -10$. The thick lines show the Local Group data for the same magnitude cuts, with the same line types (the $M_V = -10$ line lies almost entirely under the $M_V = -9$ line). *Lower right-hand panel:* as upper right-hand panel for the standard model, but with different values of R_c^0/R_{vir} (as given in the legend); R_c^0/R_{vir} is the model parameter that controls the initial orbital radii of satellites as defined in Paper I.

photon escape fraction. The result of assuming $f_{esc} = 10$ per cent (instead of $f_{esc} = 100$ per cent as in the standard model) is illustrated by the dot-dashed line in the upper right-hand panel. The number of satellites with $V_c \lesssim 30\,km\,s^{-1}$ is increased by about 10–20 per cent in the latter case.

The lower left-hand panel, shows that adopting a magnitude cut at $M_V = -10$ in the comparison produces equally good agreement (except, perhaps, at the lowest circular velocities, $\lesssim 15\,km\,s^{-1}$), but taking $M_V = -8$ leads to roughly twice as many satellites in the range $1 \lesssim V_c \lesssim 25\,km\,s^{-1}$, as is observed. In all cases, the photoionization model predicts far fewer satellites than the Cole et al. (2000) model.

Finally, we show in the lower right-hand panel of Fig. 6 the effect of varying the ratio R_c^0/R_{vir}, which parametrizes the initial orbital energy of a satellite in terms of the energy of a circular orbit

of radius R_c^0. In Paper I we demonstrated that a value of $R_c^0/R_{vir} = 0.5$ provides a good match to the number of subhaloes seen in high-resolution N-body simulations, and is comparable to the mean value measured for satellites in those simulations at $z = 0$. Increasing R_c^0/R_{vir} to 0.75 produces somewhat too many satellites, while reducing it to 0.25 seriously underpredicts the number of satellites. Increasing R_c^0/R_{vir} makes satellites orbits begin at larger radii where tidal forces are weaker, and so allows more satellites to survive (decreasing R_c^0/R_{vir} has the opposite effect). The magnitude of the changes induced by adopting these alternative values for R_c^0/R_{vir} is comparable to that seen for calculations of satellite halo abundances in the pure dark matter calculations reported in Paper I, and so can be seen to be due almost entirely to the enhanced (reduced) tidal limitation and dynamical friction resulting from a smaller (larger) value of R_c^0/R_{vir}, in combination with the changes

in the luminosities of satellites which affect whether or not they meet our selection criteria for this figure.

The exact distribution of R_c^0/R_{vir} is therefore very important, and would be worth determining accurately from numerical simulations. We stress that the value $R_c^0/R_{vir} = 0.5$ was chosen to match the results of N-body simulations of dark matter, and also results in good agreement with the abundances of satellite galaxies.

4   OTHER PROPERTIES OF SATELLITES

In addition to the abundance, our model of galaxy formation predicts many other properties of the satellite galaxy population and their associated dark haloes. We now explore some of them, particularly those for which observational data are available.

4.1   Gas content, star formation rates, metallicities and colours

We begin by considering the gaseous content and star formation rates of satellites. The mass of hydrogen (atomic plus molecular), normalized to the V-band luminosity, is shown, as a function of V-band magnitude, in Fig. 7. A rapid decline in the gas content towards faint magnitudes is predicted by the models. This is a direct consequence of the strong effects of supernova feedback in faint, low-mass galaxies which efficiently eject much of their cold gas and rapidly consume any remaining fuel (these galaxies, being satellites, are unable to accrete fresh gas in our model). The observational data show a band of almost constant gas-to-luminosity ratio which is occupied exclusively by galaxies beyond
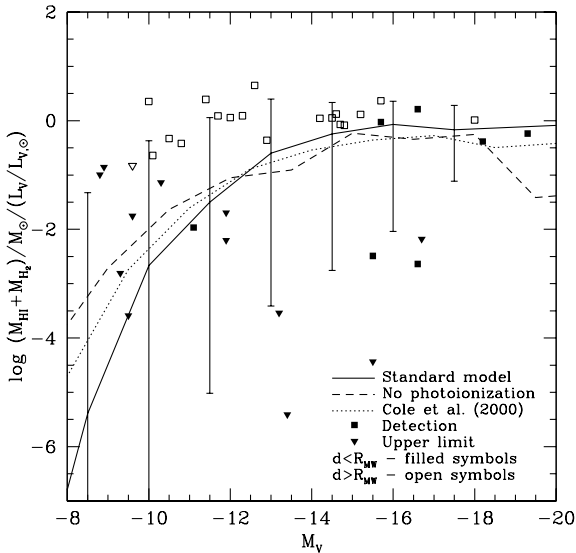
R_{MW} of the Milky Way or M31 at faint magnitudes. Galaxies within R_{MW} frequently have only upper limits to their gas mass. Our model predictions are consistent with the observations but, since the data often consist only of upper limits, this comparison is not particularly conclusive.

We now consider the star formation rates in satellites as estimated from their Hα luminosities. In Fig. 8 we plot the Hα luminosity per unit hydrogen mass for satellites with measurements or limits on Hα (all such galaxies also have measured gas masses). With so few data points (note that many of the galaxies in the plot lie further than R_{MW} from the Milky Way or M31), it is difficult to quantify the level of agreement between model and data. Of the six satellites within R_{MW} with measured Hα luminosity, four lie close to the model prediction, while one fainter satellite has an Hα-to-hydrogen ratio an order of magnitude above the model relation, and another has an upper limit lying three orders of magnitude below the model expectation.

In Fig. 9 we plot the metallicity of the ISM gas (upper panel) and of the stars (lower panel). In both cases, the Local Group satellites exhibit a trend of increasing metallicity with luminosity. Our models show a trend in the same sense, although for the ISM it appears somewhat weaker than for the data. It is interesting that the satellites within R_{MW} lie much closer to the model predictions (which are only for satellites within Milky Way-like haloes) than those outside R_{MW}, but with the limited data available it is impossible to say if this is a significant effect. The stellar metallicities in the model also agree well with the data, except perhaps at the faintest magnitudes where the model is slightly too high. While photoionization makes little difference to the metallicities of galaxies brighter than $M_V \approx -15$, at fainter
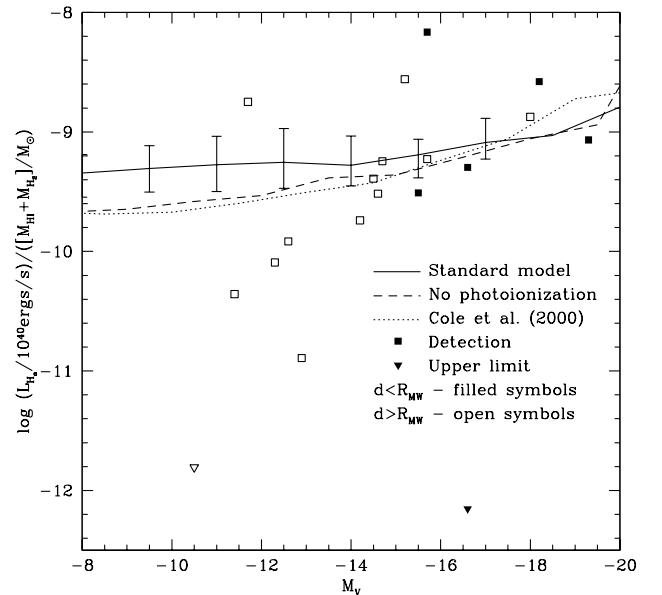

Figure 7. The mass of hydrogen per unit V-band luminosity in satellite galaxies as a function of V-band absolute magnitude. Data for the Local Group satellites are taken from Mateo (1998), except for the LMC and SMC for which H I masses are taken from Westerlund (1997), M33 for which the H I mass comes from Corbelli & Salucci (2000), and NGC 3109 and Antlia for which H I masses are taken from Barnes & de Blok (2001). H I detections are shown as squares, and upper limits as triangles. Galaxies within R_{MW} of the Milky Way or M31 are represented by filled symbols, and more distant satellites by open symbols. Solid, dashed and dotted lines show results from our standard, no-photoionization and Cole et al. (2000) models respectively. The lines show the median model relations, and the error bars indicate the 10 and 90 per cent intervals of the distribution in the standard model. The scatter in the other models is comparable to this.

Figure 8. The Hα luminosity per unit mass of hydrogen for satellite galaxies, as a function of absolute V-band magnitude. Symbols show values for Local Group satellites taken from Westerlund (1997) and Mateo (1998) for the Magellanic Clouds, and from Kennicutt (1998) for M33. Satellites within R_{MW} of the Milky Way or M31 are shown as filled symbols, with more distant satellites shown as open symbols. Hα detections are denoted by squares, and upper limits by triangles. Solid, dashed and dotted lines indicate results from our standard, no-photoionization and Cole et al. (2000) models respectively. The lines indicate the median relation, and the error bars the 10 and 90 per cent intervals of the distribution in the standard model. The scatter in the other models is comparable to this.
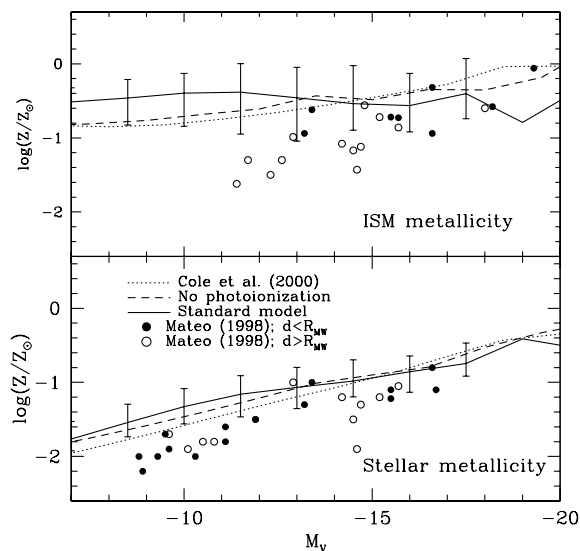
Figure 9. The metallicity of satellite galaxies as a function of absolute *V*-band magnitude. Metallicities for Local Group satellites are taken from Mateo (1998), except for the Magellanic Clouds (Skillman, Kennicut & Hodge 1989) and M33 (Kobulnicky, Kennicutt & Pizagno 1999). The upper panel shows the metallicity of gas in the ISM (relative to solar, with $Z_\odot = 0.02$), while the lower panel shows the metallicity of the stars. Filled circles indicate satellites within $R_{MW} \approx 270$ kpc of the Milky Way or M31, with more distant satellites shown as open circles. Solid lines give the median relation in our standard model, with error bars indicating the 10 and 90 per cent intervals. Dashed lines correspond to our no-photoionization model (which includes tidal stripping of satellites), and dotted lines to the Cole et al. (2000) model. The scatter in these models is comparable to that in the standard model.
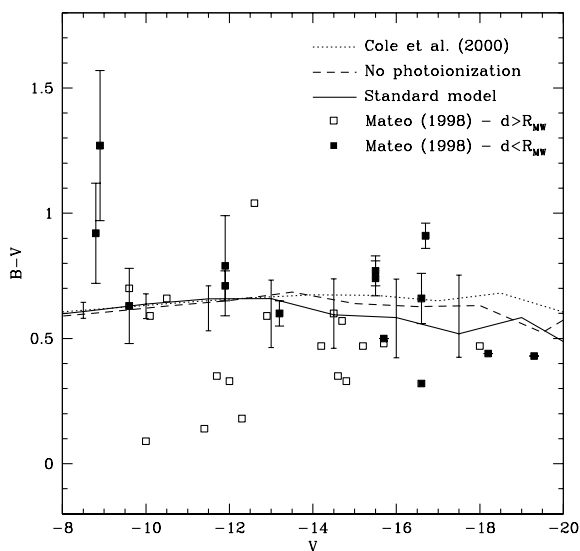

Figure 10. The $B - V$ colour of satellite galaxies as a function of absolute *V*-band magnitude. Colours for Local Group satellites are taken from Mateo (1998), except for the Magellanic Clouds (Skillman, Kennicut & Hodge 1989) and M33 (Kobulnicky et al. 1999). Filled squares indicate satellites within $R_{MW} \approx 270$ kpc of the Milky Way or M31, with more distant satellites shown as open squares. The solid line gives the median relation in our standard model, with error bars indicating the 10 and 90 per cent intervals. The dashed line corresponds to our no-photoionization model (which includes tidal stripping of satellites), and the dotted line to the Cole et al. (2000) model. The scatter in these models is comparable to that in the standard model.

magnitudes the standard model predicts slightly higher metallicities than the Cole et al. (2000) model. Photoionization causes galaxies, of a given absolute magnitude to form in higher circular velocity haloes. These have deeper potential wells which reduce the effectiveness with which supernovae feedback expels gas, thus increasing the effective yield (see Cole et al. 2000) and resulting in a higher metallicity. In Paper I we considered the metallicity of the ISM for galaxies in general, and found that photoionization actually reduced the gas metallicity in faint galaxies by preventing pre-processing of that gas in smaller haloes. In the case of satellites, photoionization has a much smaller effect because, unlike central galaxies, the satellites are not accreting gas at present, and so their metallicity is much less sensitive to any pre-enrichment.

Finally, we consider the $B - V$ colours of satellite galaxies. These are plotted in Fig. 10 for the Local Group, as a function of satellite *V*-band absolute magnitude and compared with the model predictions. The model predictions are rather insensitive to whether or not photoionization is included. With or without photoionization, satellites are typically very old systems with little recent star formation, and so their colours correspond to those of an old ($\gtrsim 10$ Gyr), low-metallicity stellar population (i.e., roughly $B - V = 0.5$–0.7 for the IMF considered here). Filled squares in the figure indicate Local Group satellites within R_{MW} of the Milky Way or M31. The colours of these galaxies are in good agreement with the model predictions, except perhaps for two intrinsically faint galaxies for which the observed colours are very uncertain. Interestingly, Local Group galaxies that lie beyond R_{MW} of either the Milky Way or M31 have systematically bluer colours, suggesting that they have experienced recent star formation. This is generically expected in our model because these objects are still the central galaxies in their host haloes and, unlike genuine satellites, they are still able to accrete gas to fuel star formation even at the present day. This interpretation is consistent with the higher overall gas content measured in the most distant galaxies, as seen in Fig. 7.

4.2 Structure

Dynamical quantities describing the structure of satellite galaxies and their dark matter haloes are readily available in our model of galaxy formation. In Fig. 11 we show some of these quantities as a function of the absolute *V*-band magnitude of the satellite. We remind the reader that in our calculations, the dynamical and structural properties of the satellite haloes within the effective tidal radius are unaffected by the mass loss beyond that radius. In the upper panels we plot the circular velocity at the virial radius (left-hand panel) and at the NFW scale radius (right-hand panel). The virial radius and corresponding circular velocity here are the values that the satellite halo last had when it was still a separate halo, before it merged with the Milky Way halo. In evaluating the circular velocity, we take into account contributions from both dark and baryonic matter in the galaxy, including the contraction of the dark halo caused by the condensation of the galaxy (which is assumed to proceed adiabatically). For fainter satellites, the photoionization model predicts significantly higher circular velocities than the other models. The reason for this is one we have encountered before: the inhibiting effect of photoionization leads to satellites of a given luminosity forming in a more massive halo than would be the case in the absence of photoionization. Note that such an effect is not seen in Fig. 5, where we plotted the satellite galaxy 'Tully–Fisher' relation. There, the increase in
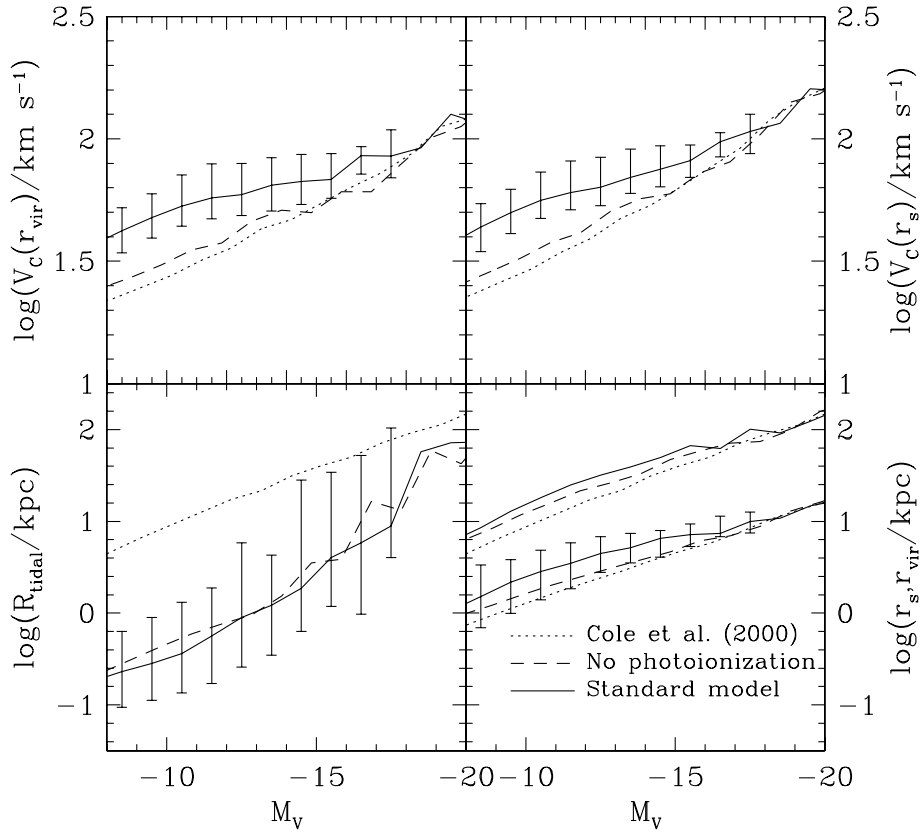
Figure 11. Predicted dynamical and structural properties of satellite galaxies and their dark matter haloes, as a function of the absolute *V*-band magnitude of the satellite. In all the panels, the lines show the median model relation: solid lines for the standard model, dashed lines for the no-photoionization model (which, however, includes tidal stripping of the satellites) and dotted lines for the Cole et al. (2000) model. As before, the error bars indicate the 10 and 90 per cent intervals of the distribution in the standard model; the scatter in the other two models is comparable. *Upper left:* The circular velocity at the virial radius. *Upper right:* The circular velocity at the NFW scale radius, r_s. This takes into account contributions from both dark and baryonic matter in the galaxy, including the contraction of the dark halo caused by the condensation of the galaxy (assumed to proceed adiabatically). *Lower left:* The effective tidal radii of the satellites. For the Cole et al. model, which does not include tidal limitation, we plot instead the virial radius of the halo for comparison. *Lower right:* The NFW scale radius of the satellite haloes (lower set of lines) and the virial radius of the haloes (upper set of lines).

circular velocity is offset by the reduction in the sizes of galaxies, which causes the visible matter to sample the rotation curve at smaller radii where the circular velocity is less.

In the lower left-hand panel of Fig. 11, we plot the effective tidal radii, as defined above and in Paper I, of the satellites.[7] For comparison, we plot the virial radius of the halo in the Cole et al. (2000) model, which does not include tidal limitation (and assumes, for calculations of dynamical friction, that the satellite retains all of its halo after it merges with a large halo). Tidal forces strip the haloes of the faintest galaxies to less than 10 per cent of their initial virial radius, but this effect becomes much less dramatic for the brighter galaxies. (The virial radii of the haloes harbouring satellites of a given M_V are actually slightly larger than the values given by the Cole et al. model, since photoionization causes galaxies of fixed M_V to form in larger haloes). In the lower right-hand panel, we show the NFW scale radius of the haloes (lower set of lines). For comparison, we also show the median virial radius (i.e., the virial radius of the satellite's halo before it merged

with the Milky Way's halo; upper set of lines). Comparison of the two shows that satellites typically formed in haloes with concentration parameters, $c = r_{vir}/r_s$, in the range $c = 5$–6.

5   DISCUSSION

Small satellite galaxies like those that surround the Milky Way are the descendants of some of the oldest objects in the Universe. Thus, to understand their properties, it is necessary to take into account processes that occurred at very early times, like the reionization of the Universe, which are often neglected when studying the properties of larger galaxies. Furthermore, since these satellites orbit in the halo of the parent galaxy, it is also important to take into account dynamical processes such as tidal effects and dynamical friction. We have used an extension of the Cole et al. (2000) semi-analytic model of galaxy formation, which includes all these processes to study the expected abundance and properties of satellite galaxies in the Local Group. Our work improves upon earlier studies by Kauffmann et al. (1993), Bullock et al. (2000) and Somerville (2001), because it self-consistently calculates the physics of reionization and galaxy formation, and includes a treatment of the main dynamical effects experienced by satellites orbiting in a dark matter halo.

We generated samples of haloes containing galaxies similar to

---

[7] In our calculations, galaxies are modelled with surface density profiles which initially extend to the virial radius of the halo in which they formed. We can therefore define a tidal radius for satellites even if this turns out to be much larger than the visible extent of the galaxy. In practice, when this occurs, the tidal radius plotted should be considered to be tidal radius of the satellite's halo rather than that of the satellite itself.

the Milky Way. Photoionization, which occurs at $z \approx 8$ for $f_{esc} = 100$ per cent, inhibits the formation of small galaxies, and so the satellites that survive to the present tend to be those that formed while the Universe was still neutral. This has the consequence of greatly suppressing the number of satellites of a given luminosity relative to the number that would be expected if photoionization were neglected. An escape fraction of $f_{esc} = 10$ per cent, which results in reionization at $z \approx 5.5$ (slightly lower than current observational limits allow), predicts around 50 per cent more galaxies at faint magnitudes ($M_V > -11$). At a given satellite luminosity, we find that it is those satellites with the lowest circular velocity that are preferentially depleted by the effects of photoionization. The measured distribution function of satellite circular velocity depends on this differential destruction, but also on the internal structure of the satellite which determines the shape of its rotation curve. We take the 'measured' circular velocity of a satellite to be the value at the half-light radius. We find that for the fainter satellites ($M_V = -10$), the measured circular velocity is about half the value at the virial radius because the half-light radius is within the rising part of the rotation curve, whereas for the brighter satellites ($M_V \simeq -15$), the measured circular velocity is very similar to the value at the virial radius. These effects work together to produce both a luminosity function and a circular velocity function that give about the observed total number of satellites. However, the shapes of the model luminosity and velocity functions appear to be somewhat too steep, so that the model underpredicts the number of bright, high-V_C galaxies. These results emerge without the need to adjust a single parameter value in the Cole et al. (2000) model nor fine-tune our treatment of photoionization. It is promising that this already reduces the total number of satellites to the observed level. The shapes of the luminosity and velocity functions can perhaps be improved by altering other parameters of the model. We defer such extensive explorations to a future paper.

Our model also predicts the sizes and metallicities of satellites, and these also turn out to be in good agreement with the limited amount of data currently available. The model predicts that photoionization has negligible effects on galaxies with circular velocity above about $60 \, \mathrm{km \, s}^{-1}$, in agreement with earlier analytical (Efstathiou 1992; Thoul & Weinberg 1996) and numerical treatments (Quinn et al. 1996; Navarro & Steinmetz 1997).

Our model can, in principle, be tested on the basis of the prediction it makes for as yet unobserved properties of the satellite population in the Local Group. In particular, our model suggests that there should be a large population of faint satellites around the Milky Way awaiting discovery. A nearly complete census would require deep imaging (at least to 26 V-band magnitudes per square arcsecond). Alternatively, satellites may be recognized as an excess of stars against the background. We have presented detailed predictions for the expected number of stars and their surface density as a function of the luminosity of the satellite to which they belong. These calculations may be useful in designing observational strategies aimed at discovering new satellites. A further possibility is to try and detect these satellites by searching for their H I content (Putman & Moore 2001). Our model predicts that $M_V = -10$ satellites should typically contain $10^5 \, \mathrm{M}_{\odot}$ of H I, with a rapid decline in H I mass at fainter magnitudes. Such observations are difficult, but perhaps not impossible.

We conclude that speculative mechanisms such as non-standard inflation (Kamionkowski & Liddle 2000) or new components of the Universe such as warm, self-interacting or annihilating dark matter (Hogan 1999; Spergel & Steinhardt 2000; Yoshida et al.

2000; Craig & Davis 2001) are not required to explain the observed abundance of Local Group satellites. Instead, the low abundance of satellites is a natural consequence of galaxy formation in a CDM universe when the physical effects of photoionization and tidal interactions, two processes which are known to occur, are taken into account. Continuing improvement in the observational data for Local Group galaxies, particularly better measurements of their structure and dynamical state and an assessment of the completeness of existing samples, together with searches for new satellites, will provide a strong test of current models of galaxy formation.

ACKNOWLEDGMENTS

REFERENCES

Abel T., Mo H., 1998, ApJ, 494, L151
Babul A., Rees M. J., 1992, MNRAS, 255, 346
Barkana R., Loeb A., 1999, ApJ, 523, 54
Barnes D. G., de Blok W. J. G., 2001, AJ, 122, 825
Baugh C. M., Cole S., Frenk C. S., 1996, MNRAS, 283, 1361
Becker R. H. et al., 2001, AJ, 122, 2850
Benson A. J., Lacey C. G., Baugh C. M., Cole S., Frenk C. S., 2002, MNRAS, 333, 156 (Paper I, this issue)
Binney J., Merrifield M., 1998, Galactic Astronomy. Princeton Univ. Press, Princeton
Bond J. R., Cole S., Efstathiou G., Kaiser N., 1991, ApJ, 379, 440
Bower R. G., 1991, MNRAS, 248, 332
Bullock J. S., Kravtsov A. V., Weinberg D. H., 2000, ApJ, 539, 517
Bullock J. S., Kolatt T. S., Sigad Y., Somerville R. S., Kravtsov A. V., Klypin A. A., Primack J. R., Dekel A., 2001, MNRAS, 321, 559
Cole S., 1991, ApJ, 367, 45
Cole S., Lacey C. G., Baugh C. M., Frenk C. S., 2000, MNRAS, 319, 168
Corbelli E., Salucci P., 2000, MNRAS, 311, 441
Craig M. W., Davis M., 2001, New Astron., 6, 425
Dehnen W., Binney J., 1998, MNRAS, 294, 429
Dekel A., Silk J., 1986, ApJ, 303, 39
Djorgovski S. G., Castro S. M., Stern D., Mahabal A., 2001, ApJ, 560, 5
Efstathiou G., 1992, MNRAS, 256, 43P
Gnedin N. Y., 2000, ApJ, 542, 535
Hogan C., 1999, in Sanchez N., Zichichi A., eds, Current Topics in Astrofundamental Physics: Primordial Cosmology. Kluwer Academic Press, Dordrecht
Irwin M., Hatzidimitriou D., 1995, MNRAS, 277, 1354
Kamionkowski M., Liddle A. R., 2000, Phys. Rev. Lett., 84, 4525
Katz N., Weinberg D. H., Hernquist L., 1996, ApJS, 105, 19
Kauffmann G., White S. D. M., Guiderdoni B., 1993, MNRAS, 264, 201
Kennicutt R. C., 1983, ApJ, 272, 54
Kennicutt R., 1998, ApJ, 498, 541
Kepner J. V., Babul A., Spergel D. N., 1997, ApJ, 487, 61
King I. R., 1966, AJ, 71, 64
Klypin A. A., Kravtsov A. V., Valenzuela O., Prada F., 1999, ApJ, 522, 82
Kobulnicky H. A., Kennicutt R. C., Pizagno J. L., 1999, ApJ, 514, 544
Lacey C. G., Silk J., 1991, ApJ, 381, 14

Leitherer C., Fergusen H., Heckman T. M., Lownethal J. D., 1995, ApJ, 454, 19

Lejeune T., Schaerer D., 2001, A&A, 366, 538

Madau P., Haardt F., Rees M. J., 1999, ApJ, 514, 648

Mateo M. L., 1998, ARA&A, 36, 435

Matthewson D. S., Ford V. L., Buchhorn M., 1992, ApJS, 81, 413

Mayer L., Governato F., Colpi M., Moore B., Quinn T., Wadsley J., Stadel J., Lake G., 2001, ApJ, 559, 754

Moore B., 2001, in Wheeler J. C., Martel H., eds, Proc. AIP Conf. Vol. 586, Proceedings of the Texas Symposium. Am. Inst. Phys., New York, p. 73

Moore B., Ghinga S., Governato F., Lake G., Quinn T., Stadel J., Tozzi P., 1999, ApJ, 524, 19

Moore B., Gelato S., Jenkins A., Pearce F. R., Quilis V., 2000, ApJ, 535, L21

Navarro J. F., Steinmetz M., 1997, ApJ, 478, 13

Navarro J. F., Frenk C. S., White S. D. M., 1997, ApJ, 490, 493

Putman M. E., Moore B., 2001, in Mulchaey J., Stocke J., eds, ASP Conf. Ser. Vol. 254, Extragalactic Gas at Low Redshifts. Astron. Soc. Pac., San Francisco, p. 245

Quinn T., Katz N., Efstathiou G., 1996, MNRAS, 278, 49

Rees M. J., 1986, MNRAS, 218, 25

Shapiro P. R., Giroux M. L., Babul A., 1994, ApJ, 427, 25

Skillman E. D., Kennicutt R. C., Hodge P. W., 1989, ApJ, 347, 875

Somerville R. S., 2001, astro-ph/0107507

Spergel D. N., Steinhardt P. J., 2000, Phys. Rev. Lett., 84, 3760

Steidel C. C., Pettini M., Adelberger K. L., 2001, ApJ, 546, 665

Taylor J. E., Babul A., 2001, ApJ, 559, 716

Thoul A. A., Weinberg D. H., 1996, ApJ, 465, 608

Weinberg M. D., Hernquist L., Katz N., 1997, ApJ, 477, 8

Westerlund B. E., 1997, The Magellanic Clouds Cambridge Astrophysics Series, No. 29. Cambridge Univ. Press, Cambridge

White S. D. M., Frenk C. S., 1991, ApJ, 379, 52

White S. D. M., Rees M. J., 1978, MNRAS, 183, 341

Yoshida N., Springel V., White S. D. M., Tormen G., 2000, ApJ, 544, L87

This paper has been typeset from a TEX/LATEX file prepared by the author.